DEBRIS VELOCITY ASSESMENT OF FIBER CONCRETE SPECIMENS LOADED BY BLAST LOAD

*Ondřej Janota, **

Katedra betonových a zděných konstrukcí, Fakulta stavební,
České vysoké učení technické v Praze, Thákurova 7/2077, 166 29 Praha 6, Česká republika.
ondrej.janota@fsv.cvut.cz

ABSTRAKT

Předmětem tohoto příspěvku je shrnutí prezentace poznatků získaných v rámci experimentu zaměřeného na stanovení výbuchové odolnosti prvků z vysokohodnotného drákobetonu (dále UHPFRC). V rámci toho experimentu byla měřena rychlost spodního povrchu jednotlivých vzorků a následně porovnána. Byly tak získány grafy vývoje rychlosti těchto povrchů v případě všech tří módů porušení (prvek bez porušení, odštěpení spodního a horního povrchu, průraz). Vývoj rychlosti spodního povrchu je v rámci toho příspěvku ukázán na třech vzorových prvcích s výše uvedenými způsoby porušení. V druhé části jsou pak naměřená data porovnána s vytvořenými numerickými modely.

KLÍČOVÁ SLOVA

Výbuchová odolnost • UHPFRC desky • rychlost výtrže• numerické modely

ABSTRACT

This paper presents overview of the experimental measurement focused on the blast resitance of the ultra-high performance fiber reinforced composited specimens. Soffit velocity measurement was performed during the experiment. These velocity measurements were performed hand in hand with the video recording of the soffit. Three typical soffit velocity developement were obtained. Each for typical failure mode (No damage, spall and crated and breach). In the second part, experimental results are compared to the numerical models.

KEYWORDS

Blast resistance • UHPFRC slabs • debris velocity • cracks

1. EXPERIMENTAL SETUP

Specimens were made of two proprietary UHPFRC materials with compressive strength 180 MPa (Premix A) and 150 MPa (Premix B). Amount and length of fibers in each concrete mixture were similar as well as other material characteristics. Specimen dimensions were 1000 x 1000 mm x 100, 150 and 200 mm. To eliminate the effect of the side reflection of pressure wave, the specimen proportions were numerically tested and evaluated as sufficient. The pressure wave reached the bottom side of the specimen and caused the damage under the blast charge sooner than it reached side sides and reflected.

To evaluate known approaches of RC and UHPFRC blast resistance prediction, different scaled distances were used for each experiment. The charge of SEMTEX 1A explosive varied from 100 g to 1000 g. Clear distance between slab's top surface and explosive varied from 0 mm (contact blast) to 100 mm (close-in blast). Each explosive was situated in the centre of the slab. Shape of the explosive was cylinder with dimeter/length ratio equal to one. The detonation point was positioned approximately 20 mm below the top surface of blast charge.

Specimens were placed on a 720 mm high steel frame (Fig. 1). On the top, three steel plates were welded peripherally to avoid falling specimen from the steel frame during the blast. Supporting of the specimens with steel frame enabled considering boundary conditions as simply supported slab in both directions.

Fig. 1*: Specimen with the explosive charge and mirror under specimen.*

2. SPALL VELOCITY DEVELOPEMENT

Spall velocity was measured by the PDV device. Results from the measurement show velocity of spalling debris (i.e. spall velocity) during blast propagation (from the initiation of blast until destruction of the collimator). Results from the PDV were divided into groups according to their final failure modes.

* Školitel: doc. Ing. Marek Foglar, Ph.D.

Three typical velocity development curves with their phenomena are presented.

In case that the failure mode was crater or no damage, then instead of spall velocity the bottom surface velocity was measured. Therefore, both collimators survived and both acceleration and deceleration of the surface were recorded. Figure 2 shows typical development of the bottom surface velocity.

Channel 1, measuring the centre of the specimen, indicated no movement until the pressure wave reached bottom surface. After that, approximately 0.14 ms after the explosion, rapid acceleration occurred. Time duration of this acceleration was almost infinitely small. After the velocity peak was reached, the surface starts to decelerate. The deceleration was, in comparison with the acceleration, gradual. Deceleration can be divided into two parts. From 0.1 ms to 0.22 ms the deceleration was slow. After that time the deceleration rate increased. Finally, bottom surface stopped moving. After that time, there was no significant movement.

Channel 2, which measured the area located 75 mm from the centre of the specimens, showed similar trend. The movement started at the exactly same time as the centre point. However, the acceleration was not so rapid, and the velocity peak was not so high. After that point the deceleration occurred. Up to approximately 0.20 ms, the deceleration rate was higher than in case of channel 1. In 0.20 ms the area started to accelerate again but the second peak value reached lower values. After the second velocity peak occurred, the surface started to decelerate again around 0.24 ms. From time 0.32 ms deceleration of both measured areas were equal. Side area measured by channel 2 stops moving in 0.5 ms.

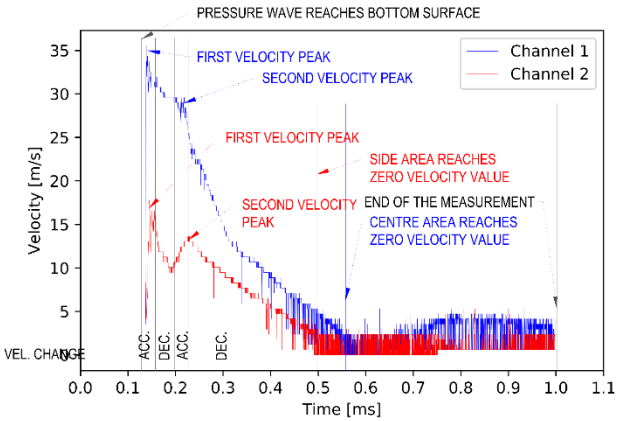

Fig. 2*: Typical bottom surface velocity for crater only/ no damage failure mode*

In case of the crater and spall failure mode was reached, the spall velocity development was similar to the development of velocity in case of only crater failure mode (Figure 3). After 0.14 ms the bottom surface started to rapidly accelerate. The velocity peak was immediately reached and the deceleration occurred. This part of deceleration lasted for about 0.15 ms and in 0.3 ms, area measured by channel two started to accelerate again. This acceleration was relatively small in comparison to main acceleration. After the second peak value was reached the area measured by channel 1 decelerated. This deceleration lasted for about 0.12 ms. Since then the velocity of centre part after the second deceleration was almost constant. However, there are parts of the curve where the velocity is constant it is not possible to precisely determine when the spall is fully ejected.

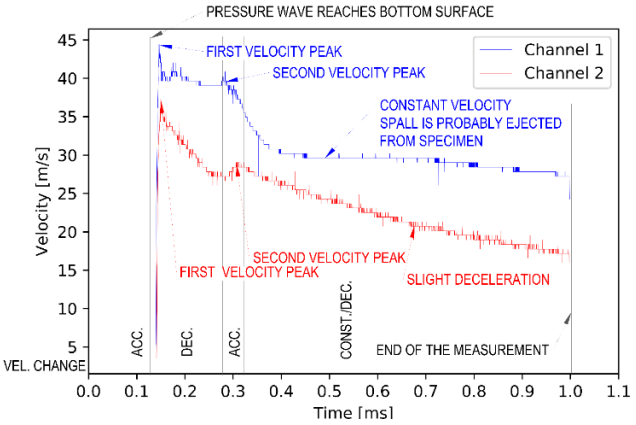

Fig. 3*: Typical spall velocity for crater and spall failure mode*

Development of spall velocity of breached specimens is relatively simple in comparison to the previous two failure modes (Figure 4). After the pressure wave reached the bottom surface, both measured areas rapidly accelerated and reached maximum velocity. Velocity of the spall was almost constant for the rest of the measurement. The measurement ended as the collimators were destroyed by the debris or measurement was manually stopped.

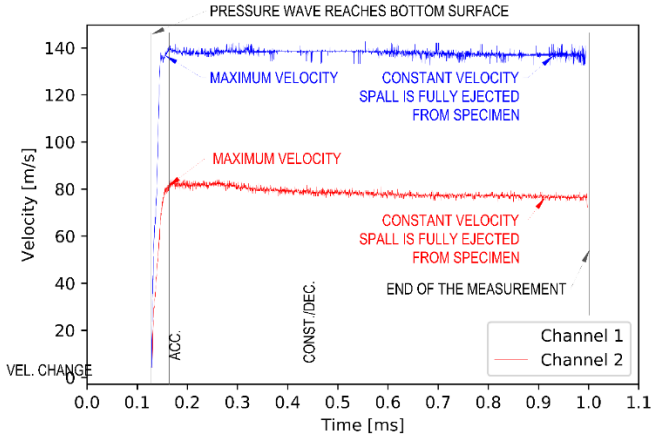

Fig. 4*: Typical spall velocity for breach failure mode*

Generally, the velocity development curve revealed following phenomena. The first velocity peak occurred immediately after the bottom surface was accelerated. This velocity was, in majority of the experimental results, the highest. In some cases, the highest velocity occurred after second or even third peak. This phenomenon can be caused by the wave reflection. If there was no spall, the bottom surface reached velocity peak and then decelerated in several phases. Each phase ended by further velocity peak. This peak, in most measurement, did not reach the values of the previous peak. Reason for this peak was probably multiple wave reflection at the edge of the specimen. Velocity development of the specimens with the crater and spall failure mode was similar to the only crater failure mode. However, in some cases the velocity stayed constant after one of the velocity peaks the ejection of the spall cannot be

determined only from PDV results. In case of breach, the curve was relatively simple. After first velocity peak was reached, the velocity did not significantly decrease and stayed almost constant for the rest of the measurement.

3. NUMERICAL MODELLING

As mentioned in the introduction, the numerical modelling of explosion experiments is intended to help understand in detail the processes that take place in the test samples. With successful numerical simulation, it is then possible to vary different material models and boundary conditions and compare the results. Currently, it is not possible to simulate blast loading in commonly used software and there is a need to use specialized software that can simulate both the behavior of common materials under blast loading and encompass the behavior of gases and energetic materials. These software include the LS-DYNA program, which is widely used for the calculation of nonlinear time-dependent problems and the simulation of fast phenomena, and was used to develop numerical models for both experiments. Two factors are then central to the correct implementation of the numerical model. The first factor is the material model, which is able to account for the behaviour of concrete/concrete wire under fast phenomena loading (material hardening and softening; strain rate effects and the associated dynamic factor increasing the strength of the material under fast phenomena loading). The second factor is the very definition of blast loading and its force.

3.1. Material model

Due to the complexity of the task, the commonly used material models are not sufficient. Determining the correct material model thus becomes one of the most complex tasks in the creation of a numerical model. Within LS-DYNA, a library of material models is available that contains multiple options to simulate the behaviour of concrete. A common problem with all the available material models is that they have all been developed to simulate plain concrete and adapting them to the behaviour of fibreconcrete is very difficult or even impossible. A widely used material model for this purpose is the MAT72_Rel3 material model (Schwer et al., 2005), (Malvar et al., 1994), (Markovich et al., 2011). MAT72_Rel3 is defined using three plastic surfaces and an equation of state, ensuring that the above phenomena are taken into account. The mathematical description of the equation of state and each surface is available to the user and their definitions can be modified. In combination with other input parameters, the openness of the model is one of the main factors why this material is used for fibreconcrete concrete simulations. In the case of developing a custom material model, two options are offered.

For commonly used concretes, it is possible to have the program generate individual parameters based on the desired strength of the concrete. The parameters obtained can then be modified to make the tensile behaviour of the material model match that of fibreconcrete or UHPC/UHPFRC. The second option is to define all the parameters yourself. Due to the number of these parameters, a significant number of tests that are not commonly used (uniaxial tensile tests, triaxial compression tests for different pressure magnitudes) are required to determine them accurately.

3.2. Blast load

The LS-DYNA software allows several approaches to model the explosion and the resulting load (pressure wave). The applicability of each method is described in detail in (Hilding, 2016). In the case of contact and very close explosion, three methods are applicable. The first is to use a Lagrangian - Eulerian (ALE) mesh of elements, cf. Fig. 5. Within this network, the Eulerian elements move freely in the Lagrangian network. This method is able to simulate the behavior of gases and materials with large deformation. A second network is then added to this network, which forms the UHPFRC plate sample itself and interacts with the Eulerian elements. The advantage of this method is the ability to observe the propagation of the explosive and the size of the pressure wave, the choice of the material model of the explosive and its equation of state. The disadvantages are, in particular, the need to create a domain that simulates the air around the test sample and the dependence of the result on the chosen shape of the Lagrangian network. This domain is needed for proper propagation of the pressure wave and expansion of the explosive. The existence of two grids led to a significant increase in the required computational time. The second approach uses the so-called meshless method (Xu et al., 2014) (Smoothed particle hydrodynamics, SPH). The explosive is not modeled by an element mesh but by particles, cf. Fig. 6. The individual particles are constrained by the material model, the equation of state and furthermore by their distance. The load is transferred to the panel by the collision of each particle with the test sample. The advantages of this approach are the reduced computational effort and computational time, the absence of a secondary mesh simulating the ambient air, and the shape variability of the explosive. The disadvantages are the dependence of the resulting load on the total number of particles and the visible discretization of the load in the case of a lower number of particles. A third approach to enable explosion modelling in LS-DYNA, is the use of an internal mechanism called the PARTICLE BLAST METHOD (PBM). This method is very similar to the second approach. The explosive is replaced by a system of particles that represent an ideal gas and behave according to Newton's laws of motion (Teng et al., 2014). The advantage of this methodology is its ease of use and very little computational effort. In the implementation it is sufficient to define the shape of the explosive, the number of particles simulating the explosive and the basic parameters of the explosive material. The disadvantages are the impossibility to define the equation of state and the limited possibility to define the material properties of the explosive.

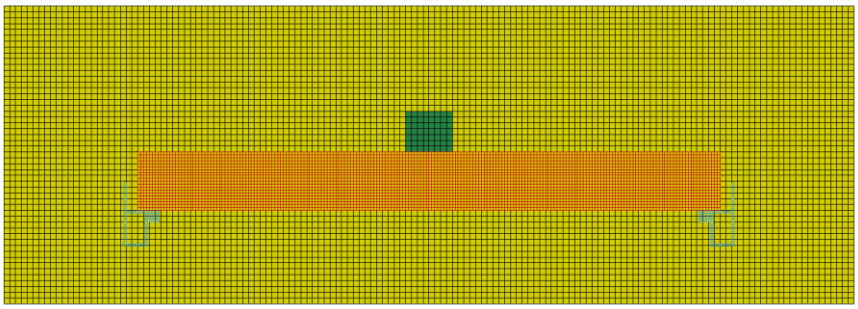

Fig. 5*: ALE model*

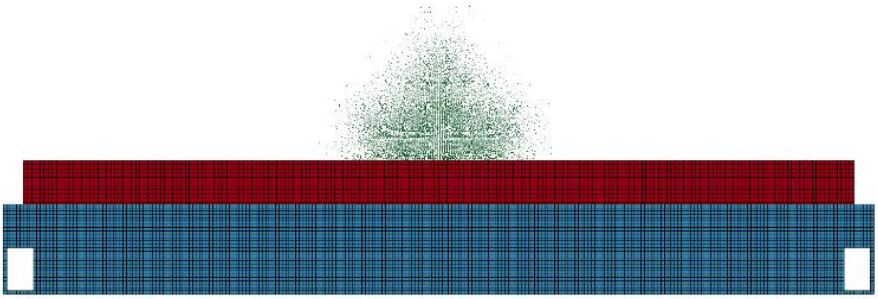

Fig. 6*: SPH model*

4. ACCURACY OF NUMERICAL MODELS

4.1. Evaluation of numerical approaches

The comparison of the different methods was made on the basis of the results obtained from the measurement of the pressure waveform on the underside of the specimen and the velocity of the bottom surface of the test specimen, see Fig. 7 and Fig. 8. The results show a very good agreement between the different methods. In the case of the bottom surface acceleration, the difference between the ALE and SPH methods is within 10%. A more pronounced difference is evident in the case of the PBM method where about 40% higher maximum velocity is achieved. Subsequently, the velocity decreases to similar values as in the case of the ALE and SPH methods. As in the case of surface velocity, the pressure evolution on the bottom surface of the test sample is similar for all three approaches. From the result, it is clear that the difference between the approaches is minimal and the methods can be considered equivalent. However, without experimental measurements of the explosive in question, it is not possible to determine the accuracy of the methods in terms of the resulting loads on the test specimens.

CONCLUSION

Two types of UHPFRC were tested for their contact and close-in blast resistance. Materials with compressive strengths 180 MPa and 150 MPa were tested. The blast loading was created using SEMTEX 1A explosive. Weight of explosive varied from 100 g up to 1000 g. The distance between top surface and the explosive charge varied from 0 to 100 mm.

Presented results in this article were focused only on the evaluation of the soffit velocity. Velocity development of three different modes of were described in detail.

Moreover three different approaches for modelling the explosion in LS-DYNA were investigated and compared in the context of numerical model building. The results show that despite the different definition of the explosive and the explosion propagation mechanism, the approaches are equivalent. The comparison of experimental and numerical results shows the accuracy of the numerical models in the case of the resulting damage and crack propagation. However, the results are burdened by the inability to simulate sample fragmentation and the unclear definition of damage. In the case of comparing an exact measured quantity, the bottom surface velocity, the numerical model shows significant shortcomings. The course of the initial acceleration is identical to the experimental results, but the same maximum velocity is not achieved in the numerical model. The following lower surface velocity waveform is completely unrepresentative. The difference is again due to the inability to account for sample fragmentation in the numerical model

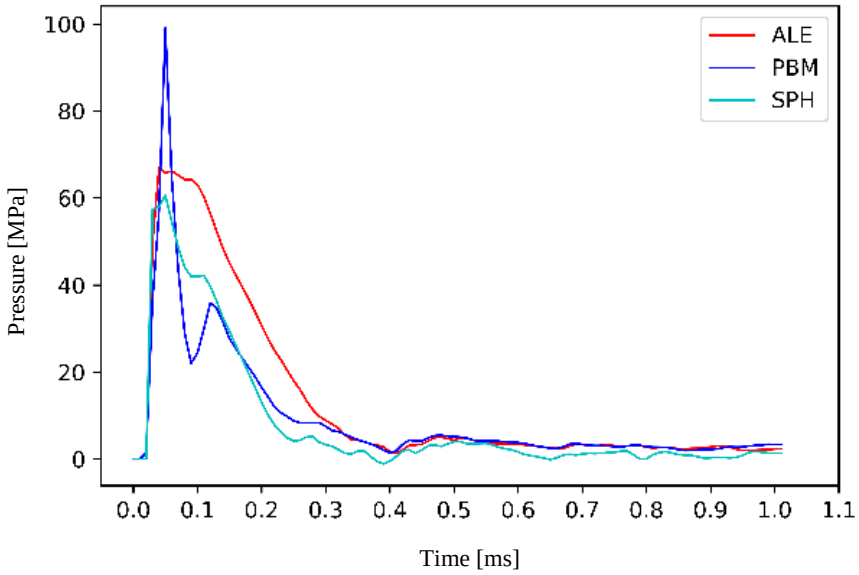

Fig. 7*: Soffit velocity*

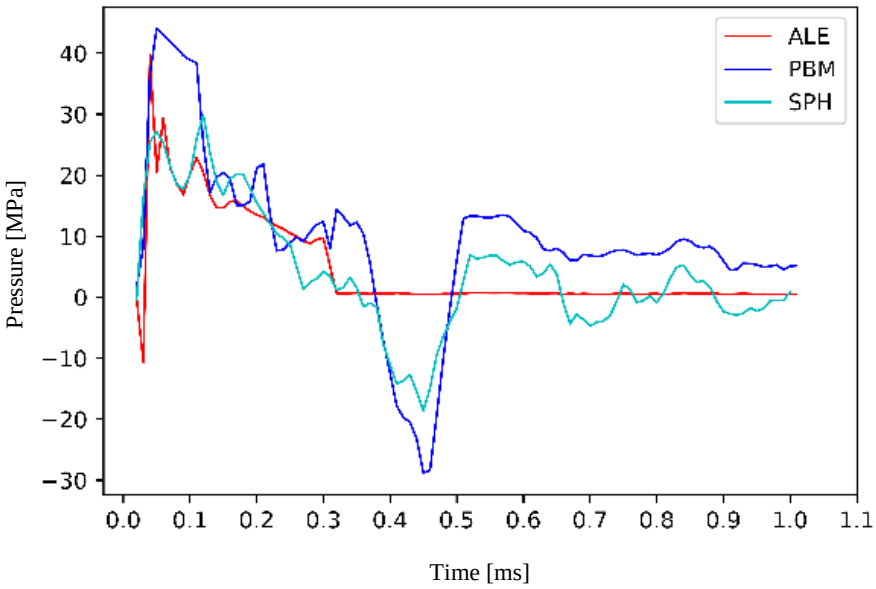

Fig. 8*: Pressure development on soffit*

ACKNOWLEDGEMENT

This work was financially supported by the Czech Technical University in Prague, project no SGS21/042/OHK1/1T/11 which is gratefully acknowledged.

References

Ahlers, Edvard B. Debri Hazards, A Fundamental Study: Final Report. IIT Research Institute, Chicago, 1990.

Cole, J. Kenneth, Larry W. Young A Terry Jordan-Culler. Hazards of Falling Debris to People, Aircraft, and Watercraft [online]. 1997 [cit. 2019-05-14].

Schwer, L. E., Malvar L.J., Simplified Concrete Modeling with *MAT_CONCRETE_DAMAGE_REL3 [online]. 2005.

Malvar L.J., Crawfor, J.E, Wesevicj, J.W. And Simons, D. A new concrete material model for DYNA36, Karagozian and Case. Report No. TR94-14.3, 1994

Markovich N., Kochaiv E., Behn-Dor G. Calibration of a Concrete Damage Material Model in LS-DYNA for a

Wide Range of Concrete Strengths, Protective Technologies Research and Development Center, Finite Elements in Analysis and Design, Volume 47, Issue 11, 1280-1290 (2011)

Hilding D., Methods for Modelling Air Blast on Structure in LS-DYNA, Nordic LS-DYNA Users‘ Conference 2016

Xu J., Wang J., Interaction Methods for the SPH Parts (Multiphase Flows, Solid Bodies) in LS-DYNA, 13th International LS-DYNA Users Conference 2014.

Teng H., Wang J., Particle Blast Method (PBM) for Simulation of Blast Loading, 13th International LS-DYNA Users Conference 2014.